Nuclear Instruments and Methods in Physics Research A 681 (2012) 68–77

Contents lists available at SciVerse ScienceDirect

Nuclear Instruments and Methods in Physics Research A

journal homepage: www.elsevier.com/locate/nima

Calibration of photomultiplier tubes for the fluorescence detector of telescope array experiment using a Rayleigh scattered laser beam

Shingo Kawana [a,*], Nobuyuki Sakurai [b], Toshihiro Fujii [b], Masaki Fukushima [c,d], Naoya Inoue [a], John N. Matthews [e], Shoichi Ogio [b], Hiroyuki Sagawa [c], Akimichi Taketa [c,f], Masato Takita [c], Stan B. Thomas [e], Hisao Tokuno [g,h], Yoshiki Tsunesada [g], Shigeharu Udo [i], Lawrence R. Wiencke [j]

[a] Graduate School of Science and Engineering, Saitama University, Saitama 338-8570, Japan
[b] Graduate School of Science, Osaka City University, Sumiyoshi, Osaka 558-8585, Japan
[c] Institute for Cosmic Ray Research, University of Tokyo, Kashiwa, Chiba 277-8582, Japan
[d] Institute for the Physics and Mathematics of the Universe, University of Tokyo, Kashiwa, Chiba 277-8582, Japan
[e] Department of Physics and High Energy Astrophysics Institute, University of Utah, Salt Lake City, UT 84112, USA
[f] Earthquake Research Institute, University of Tokyo, Bunkyo-ku, Tokyo 113-0032, Japan
[g] Graduate School of Science and Engineering, Tokyo Institute of Technology, Meguro, Tokyo 152-8551, Japan
[h] Interactive Research Center of Science, Graduate School of Science and Engineering, Tokyo Institute of Technology, Meguro, Tokyo 152-8551, Japan
[i] Kanagawa University, Yokohama, Kanagawa 221-8624, Japan
[j] Department of Physics, Colorado School of Mines, Golden, CO 80401, USA

ARTICLE INFO

Article history:
Received 18 September 2011
Received in revised form
23 February 2012
Accepted 4 March 2012
Available online 1 April 2012

Keywords:
Ultra-high energy cosmic ray
Air fluorescence telescope
Calibration of photomultiplier
Rayleigh scattering

ABSTRACT

We performed photometric calibration of the PhotoMultiplier Tube (PMT) and readout electronics used for the new fluorescence detectors of the Telescope Array (TA) experiment using Rayleigh scattered photons from a pulsed nitrogen laser beam. The experimental setup, measurement procedure, and results of calibration are described. The total systematic uncertainty of the calibration is estimated to be 7.2%. An additional uncertainty of 3.7% is introduced by the transport of the calibrated PMTs from the laboratory to the TA experimental site.

1. Introduction

The Telescope Array (TA) experiment is designed to observe extensive air showers caused by Ultra-High Energy Cosmic Rays (UHECRs), using air fluorescence telescopes and an air shower array installed in the west desert of Utah, USA [1,2]. An important scientific objective of the TA experiment is to measure the energy spectrum of cosmic rays in the ultra-high energy region, where a cutoff structure generated by the interaction of UHECRs with the cosmic microwave background has been predicted by Greissen, Zatsepin and Kuzmin (GZK) [3,4].

A measurement reported by the AGASA experiment in 1998 showed a spectrum that extended beyond the expected GZK cutoff [5,6]. The HiRes experiment recently reported a strong suppression of cosmic ray flux [7] at around the predicted energy of $10^{19.7}$ eV [8], which was also observed by the Pierre Auger Observatory [9].

A precise measurement of the cutoff energy and the spectral shape around the cutoff is crucial to the identification of the origin of the observed structure, i.e., whether it is caused by the GZK effect or by some other mechanism such as the acceleration limit of cosmic rays. Answering this question is an important objective of the TA experiment.

The TA consists of two different types of detectors. An air shower array covers a ground area of about 700 km^2 with 507 scintillator Surface Detectors (SDs) deployed in a grid of 1.2 km spacing. The spectral shape of UHECRs can be measured with good accuracy by the SD. It is fully efficient for the trigger and event reconstruction above $10^{18.8}$ eV. Three Fluorescence Detector (FD) stations, each with 12–14 fluorescence telescopes, view the sky over the surface array from the periphery (Fig. 1). The energies of UHECR events can be reliably determined by the FD because it directly measures the energy deposit in the atmosphere generated by air showers.

The energy determination by the FD is affected by several experimental uncertainties such as the fluorescence spectrum and yield, the atmospheric attenuation of fluorescence photons, the photometric calibration of the telescope, and the missing

* Corresponding author.
E-mail address: kawana@crsgm1.crinoue.phy.saitama-u.ac.jp (S. Kawana).

0168-9002/$ - see front matter © 2012 Published by Elsevier B.V.
http://dx.doi.org/10.1016/j.nima.2012.03.011

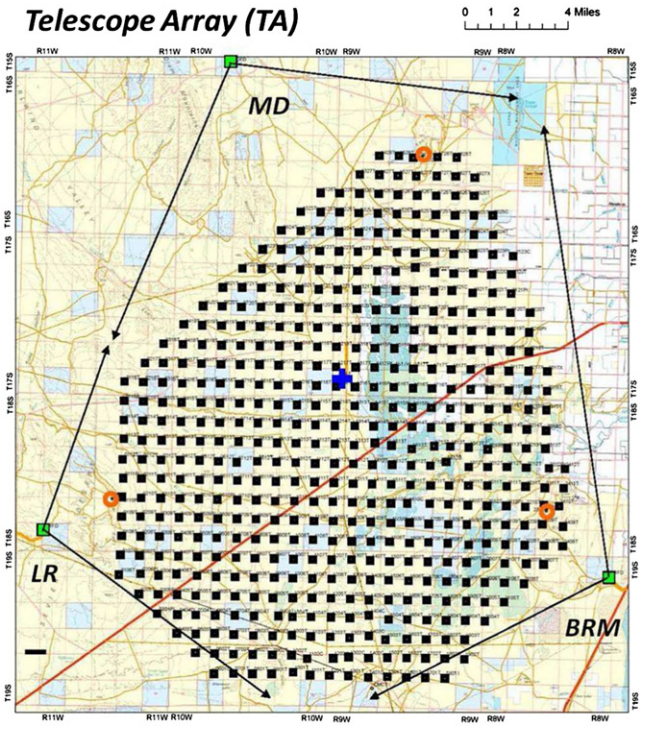

Fig. 1. Detector layout of the TA experiment. The filled squares indicate the locations of the SDs. Three hollow squares, forming a triangle surrounding the SD array, show the locations of the FD telescope stations; the extent of their azimuthal field of view is indicated by arrows.

energy carried away by high energy muons and neutrinos. In this paper, we address the third uncertainty, i.e., the photometric calibration of the PMTs used for the FD camera.

One of the three FD stations of the TA, Middle Drum (MD), is located to the north of the SD array (Fig. 1). The telescopes at the MD site are refurbished HiRes [10] telescopes. A calibration procedure similar to that employed by HiRes using a xenon flasher was applied to the FDs in MD. The role of MD is to import the established energy scale of previous experiments (HiRes-1, HiRes-2, and Fly's Eye) to the TA.

The other two FD stations, i.e., Black Rock Mesa (BRM) in the southeast and Long Ridge (LR) in the southwest, were newly produced for the TA experiment [11]. A spherical mirror (diameter 3.3 m) and an imaging camera (16×16 PMT matrix) are installed in the FDs of BRM and LR. The field of view of one telescope is 18° in azimuth and 15.5° in elevation. A combination of 6×2 telescopes at each station provides a field of view of 108° in azimuth and $3–33^\circ$ in elevation.

For the new telescopes at BRM and LR, we calibrated a combination of PMT and readout electronics using a pulsed UV light source developed specially for this purpose. This system is composed of a pulsed nitrogen laser and a gas-filled chamber in which laser photons are scattered by the gas molecules and detected by a PMT to be calibrated. We call it CRAYS (Calibration using RAYleigh Scattering). In this paper, we describe the development of CRAYS and the absolute photometric calibration of the FD camera PMTs via CRAYS.

2. FD camera and its calibration

A photograph of the PMT assembly used for the FD camera is shown in Fig. 2. The PMT (R9508, Hamamatsu Photonics) has a hexagonal photo-sensitive window with the opposite side distance of 60 mm. The PMT has a typical quantum efficiency of 27%

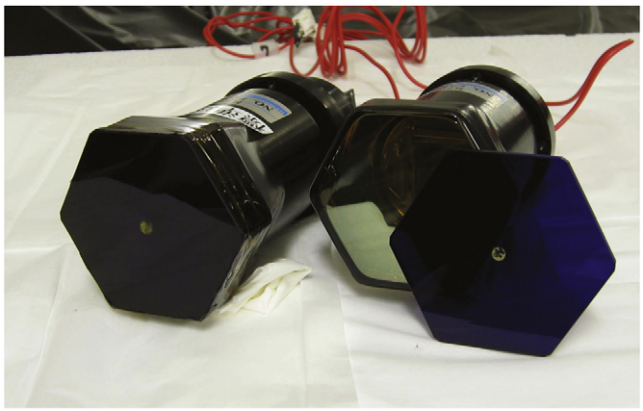

Fig. 2. PMT assembly of the TA's new FD cameras calibrated by CRAYS. The BG3 filter contacts the PMT glass window with a thin air gap. On the right, the BG3 filter is removed from the PMT. An embedded YAP pulser can be seen at the center of the BG3 filter.

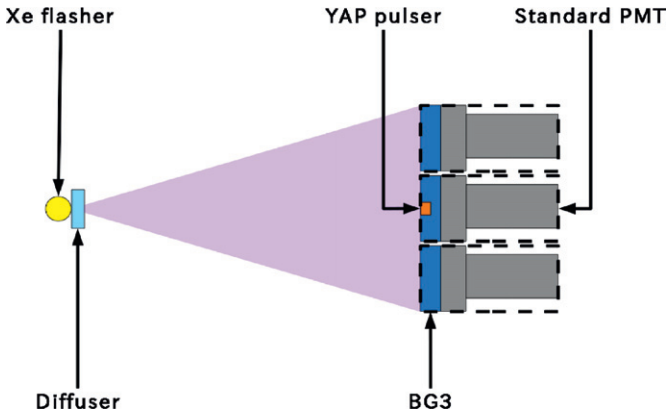

Fig. 3. Schematics of the FD camera calibration at the TA experimental site. All the 256 PMTs in each camera were illuminated by the diffused xenon flasher. Only three PMTs were drawn in the schematics for simplicity.

for $\lambda = 337.1$ nm (the laser wavelength) and a collection efficiency of 90% as reported by the manufacturer. The gains of all the PMTs were adjusted at $\sim 6.0 \times 10^4$ as described later in this paper. A UV transparent filter (BG3, Schott AG) of 4 mm thickness is attached to the PMT window. Its transmittance is measured to be 89% for $\lambda = 337$ nm [12].

The signal from the PMT is amplified by a factor of 52.7 at the PMT base and is sent to a Signal Digitizer and Finder (SDF) module [13] using a 25 m long twisted pair cable. The waveform is digitized by a 12-bit, 40 MHz Flash ADC (FADC) with 2.0 V full scale. Four consecutive digitizations of the same input signal are summed together by the Field Programmable Gate Array (FPGA) in the SDF, and the data of 14-bit dynamic range is read out.

The overall schematics of the FD PMT calibration at the TA is shown in Fig. 3. We calibrated 75 PMTs using CRAYS in a laboratory at the Institute for Cosmic Ray Research (ICRR), University of Tokyo, in Japan. The CRAYS-calibrated PMTs were transported to the TA experimental site in Utah, and installed into the FD cameras—one calibrated PMT at the center of each camera (Standard PMT) and another calibrated PMT toward the corner of the camera to monitor the behavior of the Standard PMT. The same High Voltage (HV), as determined by the CRAYS calibration at the ICRR, was applied to the Standard PMT at the TA site. Using a diffused xenon flasher [12] in situ, we adjusted the HVs of all other PMTs (255 units) in the camera such that the gains of these PMTs are equal to the Standard PMT.

All the PMTs calibrated via CRAYS have a small YAP light pulser (diameter 4 mm) [14] embedded in a hole at the center of the BG3 filter (Fig. 2). The YAP is composed of a $YAlO_3$:Ce scintillator with 50 Bq of ^{241}Am applied on the surface. The YAP generates a light flash (wavelength $\sim$350 nm; duration $\sim$30 ns) and produces approximately 450 photoelectrons in the PMT. The gains of the PMTs calibrated via CRAYS in the laboratory have been monitored in the field using the YAP signal.

3. CRAYS

The setup of CRAYS is shown in Fig. 4. A pulsed laser beam is directed into a scattering chamber filled with a high purity gas ($>$99.999%) consisting of a single molecular species, either N_2 or Ar. Scattered photons from the beam illuminate a PMT viewing the chamber through a window. Since the gas is very pure and the molecules in the gas are much smaller than the wavelength used, the scattering process in the chamber is well described by molecular (Rayleigh) scattering. The total number of photons in the laser pulse is calculated from the energy measured by a calibrated energy probe at the end of the beam line. The number of the Rayleigh scattered photons is calculated using the cross-section formula, which has been experimentally verified to an accuracy of $\sim$1% [15] (Section 8.1). With a typical setup of CRAYS for nitrogen gas (laser intensity 200 nJ; gas pressure 1000 hPa), an intensity of approximately 80 photons/cm^2 is obtained on the PMT window (Section 6.1). Uncertainties of the CRAYS calibration are 0.3% (statistical), 7.2% (systematic), and 3.7% (from transport to TA site) as described in Section 8. We note that the same CRAYS setup was also used with much lower laser intensity for calibrating the IceCube PMTs in single photon counting mode [16].

3.1. Light source and optics

We used a nitrogen laser (VSL-337ND-S, Laser Science, Inc.) as a light source (wavelength 337.1 nm; duration 4 ns). The maximum energy is 300 μJ per pulse. The wavelength of the nitrogen laser matches that of the brightest air fluorescence line in the atmosphere [17]. The diameter of the laser beam was limited to $\sim$1 mm by a set of irises at the exit of the laser and at the entrance of the scattering chamber. A remote-controlled shutter in the beam line prevented the laser light from entering the chamber, as required. A Neutral Density (ND) filter was used to reduce the beam intensity. The reflected beam by the ND filter was measured by a pyro-electric energy probe (Rjp-435, Laser Probe, Inc.) that monitored the relative intensity of the beam.

The nitrogen laser is inherently depolarized. To eliminate an elliptical polarization introduced by the ND filter, a combination of a polarizer and a retardation plate ($\lambda/4$) was used to convert the beam into a circular polarization. The intensity of the beam in the scattering chamber was measured using a silicon photodiode energy probe (Rjp-465, Laser Probe, Inc.) placed at the end of the beam line. Both energy probes were calibrated with 5% absolute accuracy by the manufacturer. The energy measured by Rjp-465 ranged from 190 nJ to 220 nJ with a typical pulse-to-pulse fluctuation of 3% as shown in Fig. 5.

3.2. Scattering chamber

The cylindrical scattering chamber has a diameter of 500 mm. The inner surface is anodized in black, and the inner wall is coated

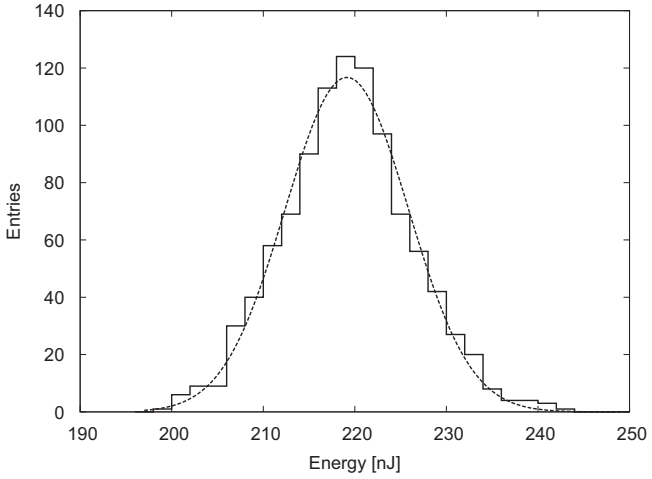

Fig. 5. Distribution of the laser energies for one calibration run. A fit to the Gaussian is shown in the dashed line (σ/peak=0.031).

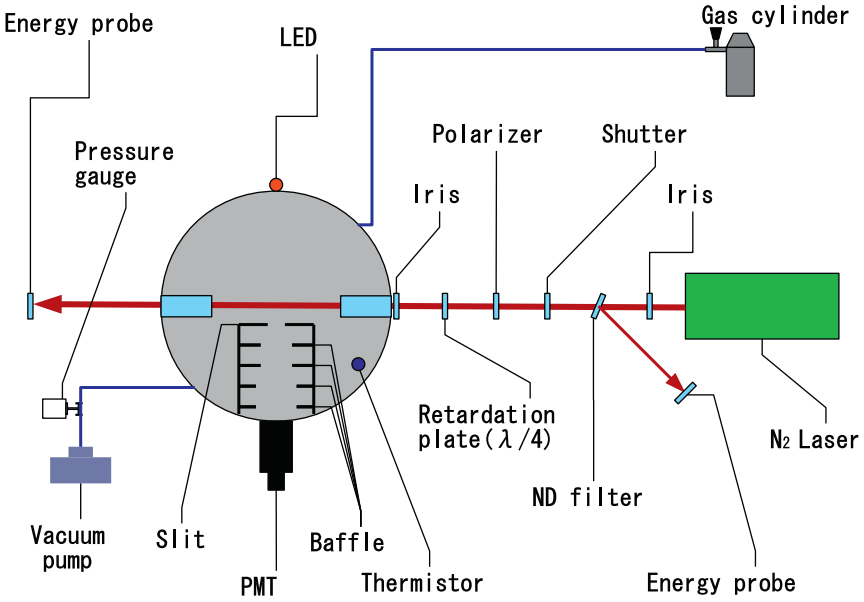

Fig. 4. Measurement setup of CRAYS.

with non-reflective black paper to suppress stray light. The chamber was evacuated to ~ 3 hPa using a membrane vacuum pump (DAU-100, ULVAC, Inc.) before introducing the high purity scatterer gas. The differential pressure of the chamber with respect to the atmospheric pressure was monitored by a capacitance manometer (BOC EDWARDS, Barocel 600AB) and the temperature inside the chamber was measured by a thermister thermometer.

The PMT to be calibrated was installed just outside the chamber, as shown in Fig. 4. The distance from the center of the chamber to the PMT glass window was set to 312 mm. The PMT detects photons scattered by the gas molecules near the center of the chamber at a scattering angle (θ) of 90°. The aperture of the PMT is limited by a slit (width 38.9 mm; height 10 mm) located 37.5 mm away from the beam line. The aperture is further limited by a removable mask installed 7 mm in front of the PMT glass window. Masks having a hole of 20.0 mm and 36.0 mm in diameter exposed only the central part of the PMT window where the uniformity is expected to be good. All chamber windows are made of CaF_2 with anti-reflection coating. A transmittance greater than 99% for $\lambda = 337$ nm was measured by the manufacturer.

3.3. Electronics and DAQ

We used the same data acquisition electronics and cables used at the TA sites as much as possible with the exception of the high voltage power supply of the PMT. We verified that the applied HVs were the same at the CRAYS calibration and at the TA sites, using a reference resistor and a digital multi-meter. Data acquisition was controlled using a PC that generated a trigger for the laser. The synchronization output of the laser was fed to the energy probes, and the energy readings of each laser shot were recorded by the PC. The pressure and the temperature of the chamber were also recorded for each calibration run.

The waveform output from the PMT was transmitted to the digitizer module (SDF) installed in a VME crate. The synchronization signal from the laser was recorded by the SDF to define the signal integration interval in the off-line analysis. For YAP data recording, a trigger was generated in the SDF by the YAP signal itself. The DAQ rate was approximately 20 Hz for the CRAYS run and 50 Hz for the YAP run.

4. Performance check

Before using CRAYS for calibration, we made the following investigations to ensure that the photons detected by the PMT originated from the Rayleigh scattering of the laser beam and that the background photon was under control. First, the polarization of the beam was measured by temporarily inserting a rotatable polarization plate and recording the output of the energy probes at different rotation angles. In Fig. 6, the relative intensity of the laser beam measured by the downstream energy probe is plotted with respect to the change of the polarizer rotation angle ϕ. A fit to the sinusoidal curve

$$1 + A \sin 2(\phi + \phi_0) \quad (1)$$

was made with an amplitude A and a phase ϕ_0 as free parameters. The obtained values, $A = -0.04$ and $\phi_0 = -8°$, indicate an elliptical polarization of 4% in the axis 37° away from the vertical-upward direction. An effect of the polarization on the number of expected Rayleigh scattered photons in the CRAYS setup is described in Section 8.2.

Next, the amount of the scattered photons and the PMT responses were measured by changing the pressure of the gas between 3 and 1013 hPa. The integration of the FADC signal and the pedestal subtraction were done in the same manner as

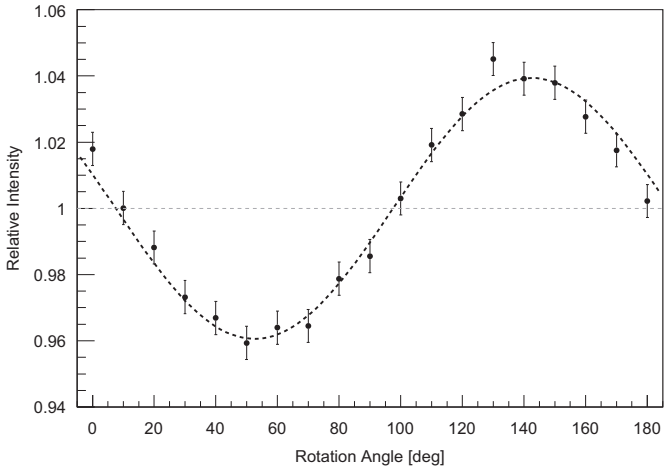

Fig. 6. Relative change of the measured laser energy with respect to the polarizer rotation angle. A fit to the sinusoidal function is shown in the dashed line.

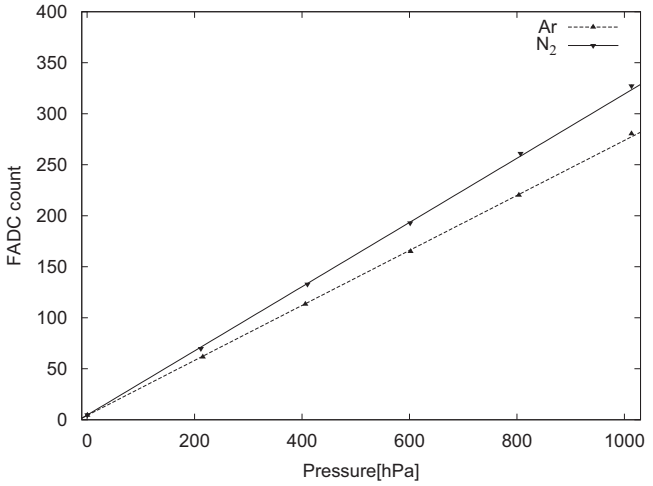

Fig. 7. Integrated FADC counts generated by the photons scattered from the laser beam with respect to the change in gas pressure. A linear fit is shown in the solid line (nitrogen) and in the dashed line (argon).

described in Sections 6.2 and 7. The result of the measurements for nitrogen and argon gas are shown in Fig. 7. Good linearities of the PMT output with respect to the change of the gas pressure were obtained both for nitrogen and argon. The argon to nitrogen ratio (Ar/N_2) was 0.857 ± 0.007 from a linear fit to the measured FADC counts and taking a ratio of the two slopes. The measured ratio is in a good agreement with the theoretical cross-section calculation, which predicts a value of 0.849 (Section 8.1).

A signal of 16-photons-equivalent was detected in the vacuum setup. This is about 1.9% of the Rayleigh scattered photons for the laser energy of 200 nJ, measured with the PMT mask of 36 mmϕ (nitrogen gas; pressure, 1000 hPa). This background without scatterer molecules in the CRAYS chamber was attributed to the stray light generated by reflection of the laser by beam line elements such as the CaF_2 window and the energy probe. The background amount was stable during the calibration runs, and its contribution to the PMT signal was subtracted in the data analysis.

Finally, a linear polarization was artificially introduced in the beam line using the rotatable polarization plate, and the PMT signal was measured for different polarization angles. The measurement was made for nitrogen gas. Fig. 8 shows a change of the integrated FADC count for different settings of the rotation angle (ϕ) of the polarization plate between 0° and 180°, where ϕ is

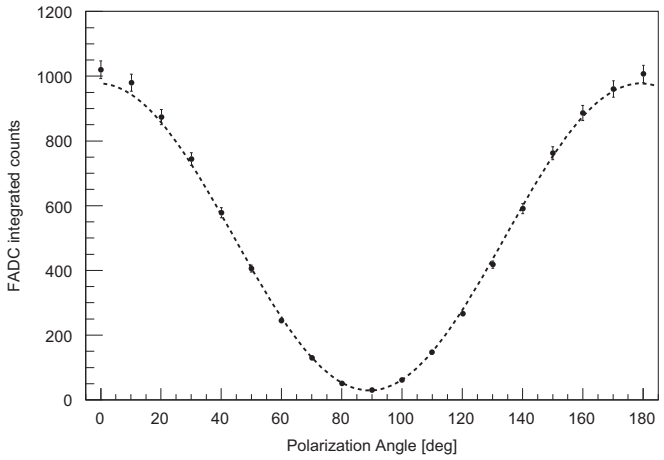

Fig. 8. Integrated FADC counts generated by the photons scattered from the polarized laser beam with respect to the change of polarization angle. A fit to the sinusoidal function is shown in the dashed line.

defined to be zero in the vertical-upward direction. The data points are fitted with a sinusoidal function [18]:

$$A\left[\frac{1+\rho_0}{2+\rho_0}-\frac{1-\rho_0}{2+\rho_0}\cos 2(\phi+\phi_0)\right]+B \quad (2)$$

where an amplitude A, a background B, and a phase ϕ_0 are free parameters, and a depolarization ratio, ρ_0, is introduced as a constant of 0.022 (Section 8). We obtained $A=980.1$, $B=8.1$, $\phi_0=-89.2^\circ$ with $\chi^2/\mathrm{NDF}=22.9/16$. The minimum value at $\phi=-\phi_0$ is 3.0% of the maximum value, which is attributed to a depolarization effect of diatomic nitrogen gas (2.2%) and the unpolarized background (0.8%).

5. Calibration procedure

We calibrated a total of 75 PMT assemblies with CRAYS. The procedure is listed as follows.

1. A relation between the PMT gain and the applied HV was measured by pulsing a UV LED, installed in the chamber opposite to the PMT (Fig. 4). A set of LED runs were carried out in a range between -700 V and -1250 V. The integrated FADC counts X and the HV setting Y are well fitted with a function $X=\alpha Y^{\beta}$, yielding a measurement of the parameter $\beta=8.1\pm 0.4$ (rms).
2. Next, several laser runs were made for each PMT to determine the HV setting for the calibration. The scattering chamber was filled with nitrogen gas ($\sim$1010 hPa) and a PMT mask (36 mmϕ) was attached. The HV to be applied to each PMT was tuned iteratively using the gain-HV relation (step-1) such that all the calibrated PMTs had approximately the same integrated FADC counts ($\sim$360 counts for a 200 nJ laser pulse). The average of the resultant HV settings for the 75 PMTs was -870 ± 50(rms) V.
3. By applying the HV determined (step-2), three CRAYS laser runs were carried out to measure the PMT response with three different PMT mask conditions: 20 mmϕ, 36 mmϕ, and no mask.
4. After the laser calibration, the YAP data was recorded with the same HV setting for future reference.

For each CRAYS run, we collected the data of 2000 laser shots: 1000 shots with shutter-open and 1000 shots with shutter-closed. We alternated the shutter status every 100 laser shots. The shutter-closed data was used to subtract the electrical noise synchronized with the laser shots. The energy probe readings were recorded for each laser shot. The temperature and pressure of the gas inside the chamber were continuously monitored. The YAP data was also taken for 2000 events.

The temperature in the laboratory where the CRAYS setup was installed was maintained at 25 ± 1 °C during the measurement, and the absolute atmospheric pressure was measured by a mercury pressure gauge for each calibration run.

6. Data analysis

6.1. Photon acceptance

The cross-section of Rayleigh scattering in nitrogen gas at $\lambda=337.1$ nm is given by the expression (Section 8.1)

$$\frac{d\sigma_R}{d\Omega}=\frac{3}{16\pi}(1+\cos^2\theta)\times 3.50\times 10^{-26}\ \mathrm{cm}^2. \quad (3)$$

The molecular density N of the scatterers can be determined from the equation of state for the ideal gas,

$$PV=NRT \quad (4)$$

where P is the pressure, V is the volume, T is the temperature (K), and R is the gas constant having a value of 8.31 J/K/mol. For nitrogen gas at 1000 hPa and 25 °C, $N=2.43\times 10^{19}\ \mathrm{cm}^{-3}$. The minor correction for Van der Waals gas can be neglected for our purpose.

A pulse of 200 nJ nitrogen laser beam includes 3.39×10^{11} photons. With a Rayleigh scattering cross-section of $3.50\times 10^{-26}\ \mathrm{cm}^2$, the number of Rayleigh scattered photons along the beam line inside the chamber is 1.43×10^7.

We performed ray tracing of Rayleigh scattered photons in the chamber in order to estimate the number of photons accepted by the PMT. The Rayleigh scattered photons were produced along the beam line with a scattering angle dependence of $1+\cos^2\theta$ and with uniform azimuthal angle dependence. The generated photons were allowed to enter the PMT directly or with one scattering on a chamber element such as the inner wall or the baffles. The shadow of the YAP embedded in the BG3 filter was also taken into account.

The ray tracing MC simulation showed that the average number of photons that reached the PMT window was 823 for nitrogen gas at 1000 hPa with a PMT mask of 36 mmϕ, and the laser intensity of 200 nJ. An effective length of 48.8 mm of the laser beam line near the chamber center was seen from the PMT. The photons entered normal to the PMT window within 8°, making a nearly uniformly irradiated circular area (diameter 36.6 mm) on the PMT window.

The effect of stray light originating from the Rayleigh scattering by the beam line was estimated by changing reflection coefficient of the chamber inner walls. We used a measured reflectivity of 0.023 for the chamber inner wall. For this value and assuming mirror scattering, three photons on average were detected after a single scattering on the chamber wall in addition to the 823 photons of direct incidence. The number was less than one when a random (isotropic) scattering was assumed. Because the scattering is expected to be close to Lambertian on the black paper covering a major part of the chamber wall, we concluded that the effect of stray light originating from the Rayleigh scattering in the beam line is negligible. The effect of multiple scattering on the chamber wall was also tested to be negligible.

6.2. Waveform integration

A typical digitized PMT waveform is shown in Fig. 9. A time interval of 51.2 μs was recorded centered on the PMT signal. The PMT signal was detected within 100 ns of the laser synchronization signal (Fig. 9). We determined the range of signal integration

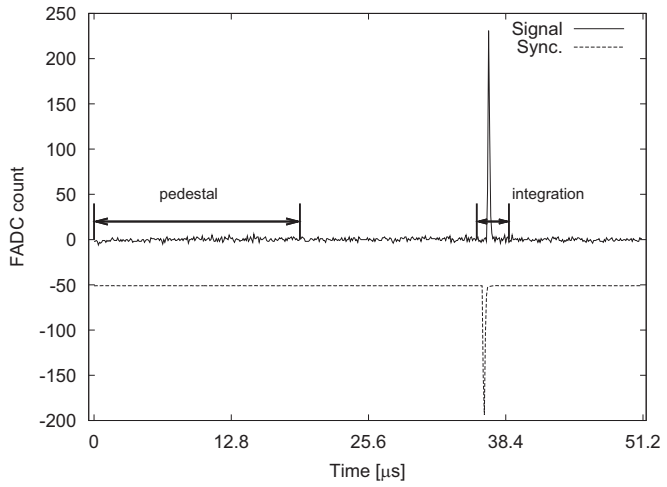

Fig. 9. Typical PMT waveform from CRAYS. The time intervals for the pedestal determination and the signal integration are indicated. The laser synchronization signal (dashed line) is inverted.

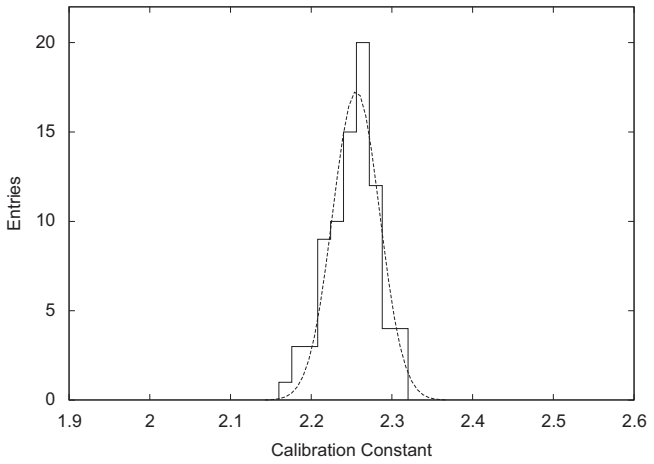

Fig. 11. Distribution of the calibration constant, C, for 75 calibrated PMTs (36 mmϕ mask). A fit to the Gaussian is shown in the dashed line (peak=2.256, $\sigma=0.0291$).

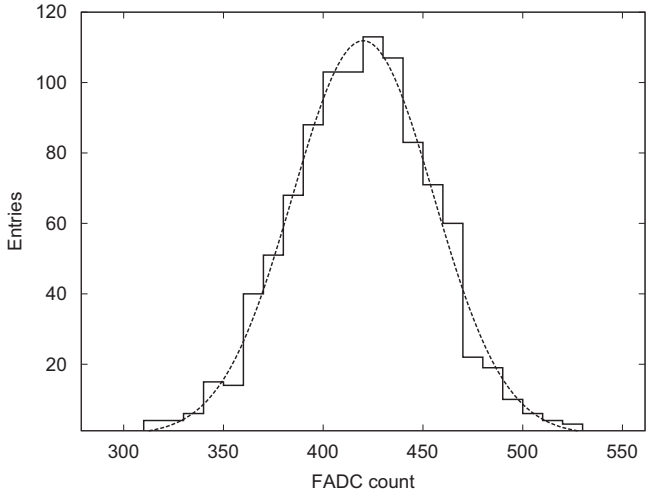

Fig. 10. Distribution of the Σ_{ADC} for a CRAYS calibration run. A fit to the Gaussian is shown in the dashed line (σ/peak=0.085).

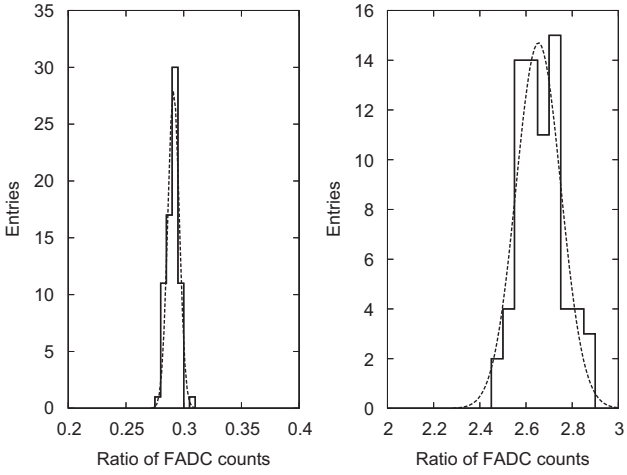

Fig. 12. Distribution of the ratio of Σ_{ADC} for 75 PMTs; 20 mmϕ-mask/36 mmϕ-mask (left) and no-mask/36 mmϕ-mask (right). A fit to the Gaussian is shown in the dashed line (peak=0.291, $\sigma=0.050$ for the left, and peak=2.65, $\sigma=0.097$ for the right).

to be 1 μs before and 2 μs after the peak of the synchronization signal. The pedestal level was evaluated as an average of 19.2 μs duration at the beginning of the recorded waveform, and it was subtracted before integration. The accidental overlap of the YAP signal in the pedestal evaluation interval was low (~0.1%), but when it happened, it was recognized by looking at the pedestal histogram, and removed.

A typical distribution of integrated PMT signals is shown in Fig. 10, after correcting the FADC signal for the shot-to-shot fluctuation in the laser energy (normalized to the average energy).

The signal resolution defined by σ/peak of the distribution is 8.5%, which is attributed to the statistical fluctuation of photoelectrons received by the first dynode (~7.0%), the single photoelectron resolution (~3%), and the electronics noise contribution (~4%).

7. Results

The photometric calibration constant C of the PMT-electronics system is defined as $C=N_\gamma/\Sigma_{ADC}$ where N_γ means the total number of photons striking the PMT sensitive area and Σ_{ADC} means the sum of the recorded FADC counts. We used the measured laser energy, gas temperature, and pressure for calculating the N_γ to be detected by the PMT. We subtracted the contribution of the shutter-closed state from the shutter-open state as a background when calculating Σ_{ADC}.

The following set of parameters were obtained for each calibrated PMT:

1. Operation HV setting.
2. Calibration constant, C, with 36 mmϕ PMT mask.
3. Σ_{ADC} with 20 mmϕ PMT mask and without PMT mask, normalized to 200 nJ laser energy.
4. Σ_{ADC} of the YAP pulser.

The distribution of C for all the 75 calibrated PMTs with 36 mmϕ PMT mask is shown in Fig. 11. The statistical accuracy of the calibration is better than 0.3%. These values are used in the air shower analysis of the TA as calibration constants. The average of 2.25 [photons/FADC count] in Fig. 11 corresponds to the PMT amplification of 6.0×10^4 using all the known optical and electrical parameters of the PMT camera system (Section 2).

The ratios of Σ_{ADC} obtained for different mask settings are shown in Fig. 12 for 75 PMTs together with the Gaussian fitting.

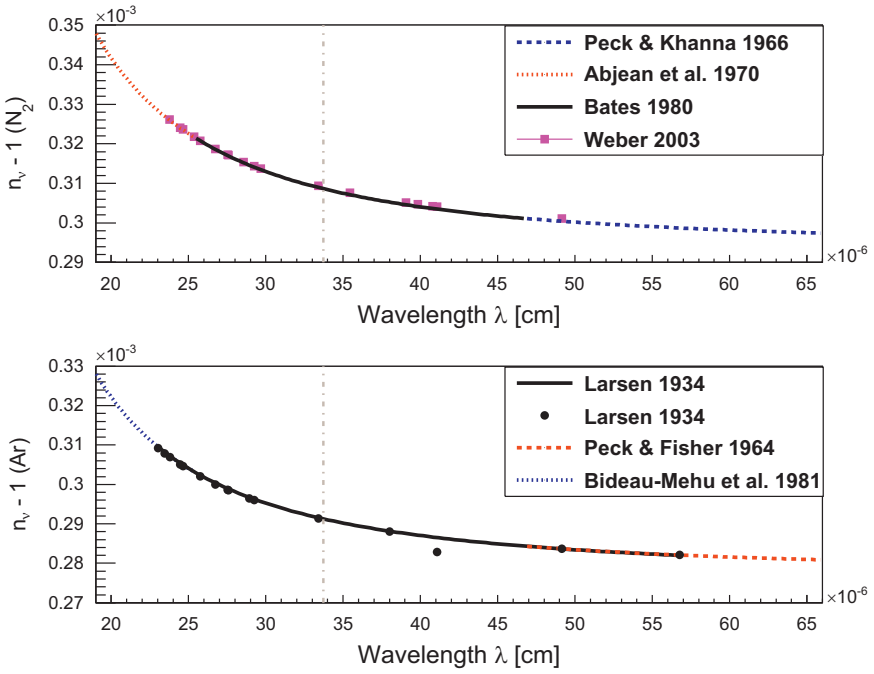

Fig. 13. Refractive indices of nitrogen (upper) and argon (lower).

The expected values of these ratios are 0.294 (20 mmϕ-mask/36 mmϕ-mask) and 2.73 (no-mask/36 mmϕ-mask) from the two-dimensional sensitivity scanning of the PMT window [12]. The fitted peaks of Fig. 12 are 0.291 and 2.65, respectively, and the measurements agreed with the expectation within 3%. The widths (σ/peak) of the two distributions, 3.4% for no-mask/36 mmϕ-mask and 1.7% for 20 mmϕ-mask/36 mmϕ-mask, indicate the level of uniformity of the photo-sensitive area among the calibrated PMTs. The accuracy of the no-mask/36 mmϕ-mask ratio is relevant for transmitting the calibration of the Standard PMT to other PMTs in a given camera, which were used for the observation without any mask, by using a diffused xenon flasher in situ.

8. Systematic uncertainties

8.1. Rayleigh scattering cross-section

The total Rayleigh scattering cross-section σ_R for a single molecule is given by (e.g. Ref. [19])

$$\sigma_R(\nu) = \frac{24\pi^3\nu^4}{N^2}\left(\frac{n_\nu^2-1}{n_\nu^2+2}\right)^2 F_K(\nu) \tag{5}$$

where ν is the wavenumber [1/wavelength], N is the molecular density, n_ν is the refractive index, and $F_K(\nu)$ is the King correction factor accounting for the anisotropy of scatterings by non-spherical molecules. In order to use Eq. (5), the values of n_ν and N should be chosen in a consistent way (i.e., values under a same condition in temperature and pressure) because of the relation $(n_\nu^2-1)/(n_\nu^2+2)\propto N$ [20]. We use n_ν values at NTP (normal temperature and pressure, $T=273.15$ K and $P=1013.25$ hPa), and we take $N=2.69\times10^{19}$ cm^{-3} [21].

Peck and Khanna [22] gave an empirical formula for the refractive index of nitrogen at NTP in the wavelength range 468–2060 nm as

$$10^8(n_\nu-1) = 6855.200 + \frac{3.243157\times10^{14}}{1.44\times10^{10}-\nu^2} \tag{6}$$

where ν is in [1/cm]. Abjean et al. [23] made a similar expression for a shorter wavelength range 181–254 nm,

$$10^8(n_\nu-1) = 6998.749 + \frac{3.233582\times10^{14}}{1.44\times10^{10}-\nu^2}. \tag{7}$$

Bates [24] gave an interpolation to cover the intermediate range for 254–468 nm in the same form as Eqs. (6) and (7) as

$$10^8(n_\nu-1) = 5989.242 + \frac{3.3632663\times10^{14}}{1.44\times10^{10}-\nu^2}. \tag{8}$$

This well reproduces the data in the literature [25] in 238–490 nm. These formulae and data are shown in Fig. 13.

Larsen [26,27] measured the refractive index of argon at NTP in 230–567 nm and gave an expression

$$\frac{3}{2}\left(\frac{n_\nu^2-1}{n_\nu^2+2}\right) = 1.2098\times10^6\left(\frac{0.208972}{0.87882\times10^{10}-\nu^2} + \frac{0.208972}{0.9100\times10^{10}-\nu^2} + \frac{4.925837}{2.69636\times10^{10}-\nu^2}\right) \tag{9}$$

where ν is in [1/cm]. This is also shown in Fig. 13, together with the measurements in different wavelength ranges given in Refs. [28,29].

The empirical formulae for n_ν of nitrogen and argon well fit the data in the wide range, including the wavelength of our interest $\lambda=337.1$ nm. For our calculation, we use Eq. (8) for nitrogen and Eq. (9) for argon, which are evaluated as $n_\nu(\mathrm{N_2})-1=3.0865\times10^{-4}$ and $n_\nu(\mathrm{Ar})-1=2.9119\times10^{-4}$, respectively.

The values of the King correction factor for nitrogen have been derived from the measurements by Bridge and Buckingham [30] and Alms et al. [31]. A widely used dispersion relation for the King correction factor of nitrogen was given by Bates [24] using these data and the calculations by Oddershede and Svendsen [32]:

$$F_K(\nu) = 1.034 + 3.17\times10^{-12}\nu^2 \tag{10}$$

where ν is in [1/cm]. Since argon is of monoatomic molecule, $F_K(\mathrm{Ar})=1$ is expected. The measurement by Rudder and Bach [33] showed that the degree of depolarization is $\sim10^{-5}$, and the deviation of $F_K(\mathrm{Ar})$ from unity is 3×10^{-5} [34,35].

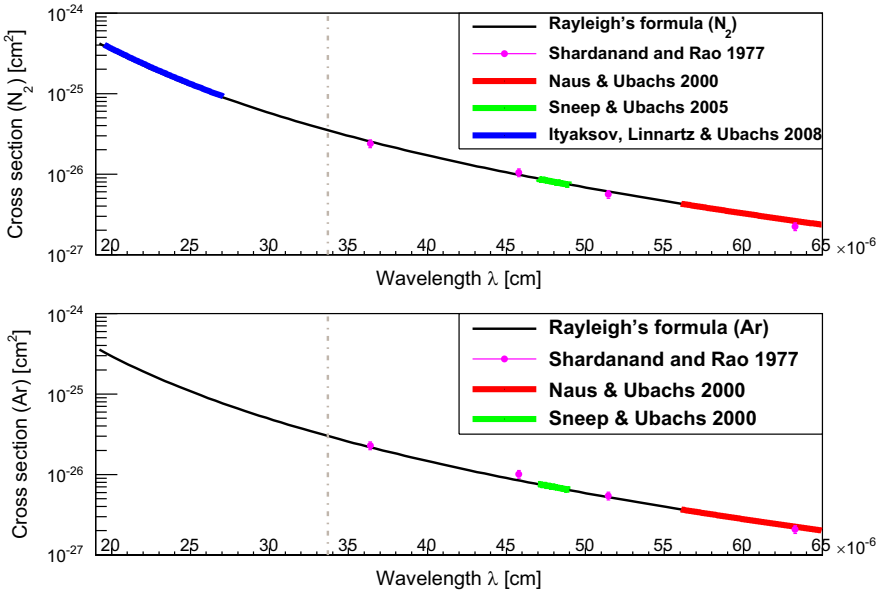

Fig. 14. Rayleigh scattering cross-sections. The solid line is calculated by formula (5) using the refractive indices and the King correction factor given in Ref. [24]. Fits for the experimental data given in the literature [15,36–39] are shown in different colors. (For interpretation of the references to color in this figure caption, the reader is referred to the web version of this article.)

Using the n_v and $F_K(\nu)$ values described above, we obtained the total Rayleigh scattering cross-sections of nitrogen and argon at $\lambda = 337.1$ nm under NTP, as

$$\sigma_R(\mathrm{N_2}) = 3.50 \times 10^{-26}\ \mathrm{cm^2}, \quad \sigma_R(\mathrm{Ar}) = 3.00 \times 10^{-26}\ \mathrm{cm^2}. \tag{11}$$

We used these cross-sections in our ray-tracing simulation of scattered laser photons in the CRAYS chamber (Eq. (3)). The accuracies of $\sigma_R(\mathrm{N_2})$ and $\sigma_R(\mathrm{Ar})$ which come from uncertainties in n_v and F_K (for nitrogen) are 1% and 0.3%, respectively (see also Ref. [15]).

The argon to nitrogen ratio is $\sigma_R(\mathrm{Ar})/\sigma_R(\mathrm{N_2}) = 0.858$. The ratio that CRAYS measures at $\theta = 90^\circ$ becomes 0.849, being slightly affected by the modification of the differential cross-section for diatomic molecules ($\mathrm{N_2}$) [18].

Experimental verifications of the Rayleigh cross-section formula (5) for gases in optical and ultraviolet wavelengths is rather scarce. An old measurement by Shardanand and Rao [36] gave cross-section values for nitrogen and argon at 5 wavelengths from 363.8 nm to 632.8 nm, which are in agreement from expectations within $1 \sim 5\%$ (Fig. 14). Naus and Ubachs firstly carried out a modern laboratory laser measurement of Rayleigh scattering cross-sections of nitrogen and argon in 560–650 nm with the cavity-ringdown technique [15,37]. They compared their measured values of cross-section and the expectations from the formula (5) with n_v evaluated with (6), (9) and $F_K(\nu)$ by (10), and concluded that the measured and the calculated cross-sections agree within an experimental uncertainty of 1%. They also gave an empirical expression for the Rayleigh cross-section in a form

$$\sigma_R(\nu) = \overline{\sigma}\nu^{4+\epsilon} \tag{12}$$

By fitting their measured values to (12) they obtained $\overline{\sigma} = 22.94 \times 10^{-45}$ and $\epsilon = 62.4 \times 10^{-3}$ for nitrogen, and $\overline{\sigma} = 19.89 \times 10^{-45}$ and $\epsilon = 61.5 \times 10^{-3}$ for argon [15]. This experiment was followed by the measurements in shorter wavelengths, as Sneep and Ubachs in 470–490 nm [38], and Ityaksov, Linnartz and Ubachs in 198–270 nm [39]. Although there are few cross-section data available in the very vicinity of our interest, $\lambda = 337.1$ nm, the measured values both in the shorter and the longer wavelength ranges are in excellent agreement with the expectation from (5) within $\sim 1\%$, and there is no evidence of non-validity of (5) at 337.1 nm.

Table 1
Systematic uncertainties of the CRAYS calibration.

	Error (%)
Cross-section (σ_R, $d\sigma_R/d\Omega$ and polarization)	2.8
Molecular density (T and P)	1.3
Measurement of laser energy	5.0
Geometric aperture calculation	3.0
Signal integration (Σ_{ADC})	2.0
Background and noise subtraction (Σ_{ADC})	1.9
Effect of geomagnetism	1.0
Total (quadratic sum of above)	7.2

8.2. Uncertainty of CRAYS

A list of systematic uncertainties for the calibration constant, C (36 mmϕ), obtained by CRAYS is given in Table 1. The calibration of PMTs with CRAYS is fully dependent on an evaluation of the total and differential cross-sections of Rayleigh scattering, σ_R and $d\sigma_R/d\Omega$, and its modification due to the polarization of the incident laser beam. As described in Section 8.1, the direct measurement of σ_R agrees with the calculation within $\sim 1\%$ in the shorter and in the longer wavelength ranges around 337.1 nm. Using CRAYS, we measured the argon-to-nitrogen ratio at $\lambda = 337.1$ nm and showed that the calculation and the measurement of the ratio agree also within 1% (Section 4). This measurement gives an additional support that our calculation of σ_R is valid at the wavelength of 337.1 nm: no unexpected phenomena (as resonant absorptions) happened to the nitrogen laser photons in nitrogen gas.

The differential cross-section, $d\sigma_R/d\Omega$, for diatomic molecules such as $\mathrm{N_2}$ is modified by a small amount from Eq. (3), which we used for estimating the number of Rayleigh-scattered photons entering the PMT (Section 6.1). This modification factor at $\theta = 90^\circ$ is $2(1+\rho_0)/(2+\rho_0)$, or 1.011 using $\rho_0 = 0.022$ for the depolarization ratio of $\mathrm{N_2}$ gas induced by the incident light of wavelength 337.1 nm. For monoatomic molecules such as argon, the depolarization ratio is zero and $d\sigma_R/d\Omega$ is calculated by Eq. (3). For nitrogen gas, we observed the depolarization effect in the CRAYS setup as described in Section 4. We assign a systematic uncertainty of $+1.1\%$ for $d\sigma_R/d\Omega$.

We observed an elliptical polarization of 4% for the incident laser beam with its polarization axis pointing 37° away from the vertical-upward direction (Section 4, Fig. 6). Rayleigh scattering of linearly polarized (100%) laser beam at $\theta = 90^\circ$ modifies the cross-section by a factor of $2(1-\cos^2\alpha)$, where α is the rotation angle of the scattered photon measured from the direction of the polarization [18]. The α is 53° for the CRAYS setup whereas $\alpha = 45^\circ$ corresponds to zero correction on the cross-section. The observed polarization of 4% gives a correction factor of 1.000 ± 0.014 on the cross-section, corresponding to $\alpha = 45^\circ \pm 10^\circ$. We assign a systematic uncertainty of 1.4% for the polarization effect.

In summary, for the systematic uncertainty of Rayleigh scattering cross-section, we have $\pm 1.0, +1.1, \pm 1.4\%$ from σ_R, $d\sigma_R/d\Omega$ and the polarization. We evaluate a total systematic uncertainty of 2.8%, taking a quadratic sum for two $\pm$ uncertainties and adding $+1.1\%$ uncertainty linearly.

The molecular density of the scatterer gas is calculated from the temperature (T) and the pressure (P) of the gas inside the CRAYS chamber. We evaluate an error of 1.3% for the molecular density calculation, consisting of the absolute calibration of the mercury barometer (0.5%), the stability of the pressure gauge calibration (1.0%), and the difference of the room temperature and the gas temperature in the scattering chamber (maximum 2 °C corresponding to 0.7%).

The largest contribution to the systematic uncertainty comes from the absolute calibration of the energy probe [40]. The manufacturer calibrated the probes with an absolute accuracy of 5% using NIST traceable standards. We used two Rjp-465 probes and the results were well within the quoted accuracy. The second largest contribution comes from the acceptance calculation, which is dominated by the measurement accuracy of the slit size (38.9 ± 0.5 mm) and the distance from the laser beam line to the PMT mask (312 ± 3 mm) including the inaccuracy of the laser beam position in the scattering chamber. We estimated a total uncertainty of the acceptance to be 3.0%.

The uncertainty of Σ_{ADC} is estimated as 2.0% from the signal integration and 1.9% from the background noise contribution. The uncertainty of signal integration (2%) is determined from the change of Σ_{ADC} by using a different method of estimating the pedestal level, and by using different signal integration intervals. The uncertainty of background and noise subtraction (1.9%) is taken from the remaining Σ_{ADC} for the zero chamber pressure run. It is a conservative estimate because the amount of the background was stable throughout the calibration, and its contribution was actually subtracted in the data analysis. An uncertainty of 1.0% was estimated for the geomagnetic effect from the change of Σ_{ADC} for the YAP run taken in different azimuthal orientations.

All added in quadrature, we determined that the total systematic uncertainty of the CRAYS calibration is 7.2%.

8.3. Transport of the calibrated PMT

Fifty PMTs with a YAP scintillator were calibrated in January 2008 in a laboratory of the Institute for Cosmic Ray Research (ICRR), University of Tokyo.[1] They were then transported to the TA site in Utah and installed in the 24 FD cameras in March 2008. Twenty two cameras had two calibrated PMTs installed and two cameras had three calibrated PMTs. The same nominal HV setting used in CRAYS calibration was applied to the Standard PMT installed at the center of the camera, and the YAP signal was measured again at the TA site. The signal obtained at the site was compared with that measured during the calibration after correcting the temperature difference, 25 °C during the calibration and ~ 10 °C at the TA site, using the temperature behavior of the YAP signal previously measured in the laboratory [41]. The result is plotted in Fig. 15 as the ratio of the two YAP measurements. Only one PMT showed a large deviation of 0.85, which is attributable to a change of the YAP light output.[2] The distribution in Fig. 15, excluding the outlier point (0.85), is fitted by a Gaussian with a mean of 0.999 and a standard deviation of 0.037. The mean value of 0.999 indicates the stability of the PMT gain from the laboratory calibration to the on-site installation. The spread of 3.7% includes all the following uncertainties and differences in the measurement: applied HVs, electronics sensitivities, temperature corrections, geomagnetic effects in Japan and Utah, and possible drifts of YAP light output and PMT gain during the transport.

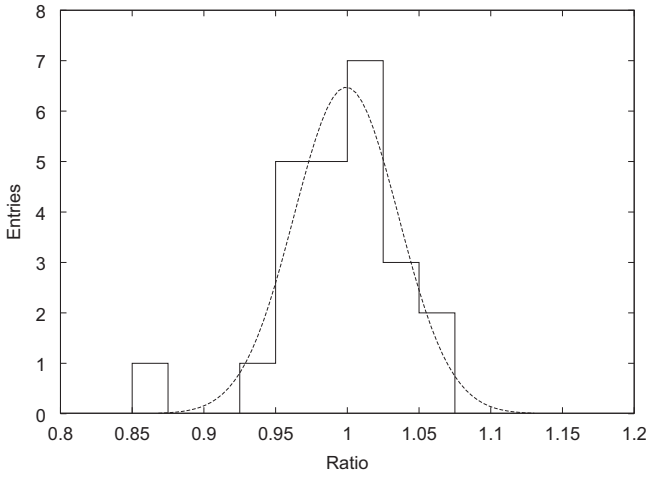

Fig. 15. Change of the YAP signal from the laboratory calibration to the on-site use. A ratio (=on-site/lab.-calib.) is plotted for 24 Standard PMTs installed in the FD camera. A fit to the Gaussian is shown in the dashed line (peak=0.999, $\sigma = 0.037$).

9. Summary

Photometric calibration of the new fluorescence telescope of the TA was carried out using CRAYS. Rayleigh scattering of nitrogen laser beam was used for CRAYS to produce a short and uniform UV light flash of known intensity on the PMT's photo-sensitive window. The Standard PMT for each FD camera was calibrated with an absolute accuracy of 7.2% via CRAYS in the laboratory. An additional uncertainty was introduced by the transport of the calibrated PMTs from CRAYS to the experimental site in Utah. It is estimated to be 3.7% using the YAP pulser.

Acknowledgments

We wish to thank the members of the Telescope Array (TA) collaboration for making it possible (and necessary) to do this study. The TA experiment is supported by the Japan Society for the Promotion of Science via Grants-in-Aid for Scientific Research on Specially Promoted Research (21000002) "Extreme Phenomena in the Universe Explored by Highest Energy Cosmic Rays," and the Inter-University Research Program of the Institute for Cosmic Ray Research; by the U.S. National Science Foundation awards PHY-0307098, PHY-0601915, PHY-0703893, PHY-0758342,

[1] A second batch of 25 PMTs were calibrated in August 2008.

[2] Another calibrated PMT installed in the same camera had the ratio of 1.007, and the gain difference of these two PMTs was 2.3% as measured by a xenon flasher run.

PHY-0848320 (Utah), and PHY-0649681 (Rutgers); by the National Research Foundation of Korea (2006-0050031, 2007-0056005, 2007-0093860, 2010-0011378, 2010-0028071, R32-10130); by the Russian Academy of Sciences (RFBR Grants 10-02-01406a and 11-02-01528a (INR)), IISN Project no. 4.4509.10; and the Belgian Science Policy under IUAP VI/11 (ULB). We also wish to thank the people and officials of Millard County, Utah, for their wholehearted support. We gratefully acknowledge the contributions from the technical staffs of our home institutions and the Center for High Performance Computing (CHPC), University of Utah.

References

[1] The Telescope Array Project: Design Report, July, 2000.
[2] H. Sagawa for the Telescope Array Collaboration, in: Proceedings of the 31st International Cosmic Ray Conference, Łódź, Poland, 2009.
[3] K. Greisen, Physical Review Letters 16 (1966) 748.
[4] T. Zatsepin, V.A. Kuzmin, JETP Letters 4 (1966) 78.
[5] M. Takeda, et al., Physical Review Letters 81 (1998) 1163.
[6] M. Takeda, et al., Astroparticle Physics 19 (2003) 447.
[7] R.U. Abbasi, et al., Physical Review Letters 100 (2008) 101101.
[8] V. Berezinsky, A. Gazizov, S. Grigorieva, Physical Review D 74 (2006) 043005.
[9] J. Abraham, et al., Physical Review Letters 101 (2008) 061101.
[10] T. Abu-Zayyad, et al., Nuclear Instruments and Methods in Physics Research Section A 450 (2000) 253.
[11] H. Tokuno, et al., Nuclear Instruments and Methods in Physics Research Section A 676 (2012) 54.
[12] H. Tokuno, et al., Nuclear Instruments and Methods in Physics Research Section A 601 (2009) 364.
[13] A. Taketa, et al., submitted for publication.
[14] M. Kobayashi, et al., Nuclear Instruments and Methods in Physics Research Section A 337 (1994) 355.
[15] H. Naus, W. Ubachs, Optics Letters 25 (2000) 347.
[16] R. Abbasi, et al., Nuclear Instruments and Methods in Physics Research Section A 618 (2010) 139.
[17] F. Arqueros, J. Hoerandel, B. Keilhauer, Nuclear Instruments and Methods in Physics Research Section A 597 (2008) 1. (and references therein).
[18] R.B. Miles, W.R. Lempert, J.N. Forkey, Measurement Science and Technology 12 (2001) R33.
[19] A. Bucholtz, Applied Optics 34 (1995) 2765.
[20] J.D. Jackson, Classical Electrodynamics, third ed., John-Wiley & Sons, 1999.
[21] P.J. Mohr, B.N. Taylor, D.B. Newell, Reviews of Modern Physics 80 (2008) 633.
[22] E.R. Peck, B.N. Khanna, Journal of the Optical Society of America 56 (1966) 1059.
[23] R. Abjean, et al., Comptes Rendus de l'Academie des Sciences B 271 (1970) 411.
[24] D.R. Bates, Planetary and Space Science 32 (1984) 785.
[25] M.J. Weber, Handbook of Optical Materials, CRC Press, 2003.
[26] T. Larsen, Zeitschrift fuer Physik 98 (1936) 17.
[27] P.J. Leonard, Atomic Data and Nuclear Data Tables 14 (1974) 21.
[28] E.R. Peck, D.J. Fisher, Journal of the Optical Society of America 56 (1964) 1362.
[29] A. Bideau-Mehu, et al., Journal of Quantitative Spectroscopy & Radiative Transfer 25 (1981) 395.
[30] N.J. Bridge, A.D. Buckingham, Proceedings of the Royal Society A 295 (1960) 424.
[31] G.R. Alms, et al., Journal of Chemical Physics 63 (1975) 3321.
[32] J. Oddershee, E.N. Svendsen, Chemical Physics 64 (1982) 359.
[33] R.R. Rudder, D.R. Bach, Journal of the Optical Society of America 58 (1968) 1260.
[34] C. Fröhlich, G.E. Shaw, Applied Optics 19 (1980) 1773.
[35] S.S. Srivastava, et al., Advances in Space Research 44 (2009) 1058.
[36] Shardanand, A.D. Rao, NASA Technical Report, NASA-TN-D-8442, 1977.
[37] H. Naus, W. Ubachs, in: Proceedings of the Lasers and Electro-Optics Europe 2000, IEEE/IET Electronic Library, 2003.
[38] M. Sneep, W. Ubachs, Journal of Quantitative Spectroscopy & Radiative Transfer 92 (2005) 293.
[39] D. Ityaksov, H. Linnartz, W. Ubachs, Molecular Physics 106 (2008) 2471.
[40] L. Wiencke, F. Arqueros, J. Compton, M. Monasor, D. Pilger, J. Rosado, in: Proceedings of the 31st International Cosmic Ray Conference, Łódź, Poland, 2009 arXiv:1105.4016 [astro-ph].
[41] S. Ogio, et al., in: Proceedings of the 31st International Cosmic Ray Conference, Łódź, Poland, 2009.